RESEARCH PAPER

Biosynthesis of $Srco_3$ nanostructures with honey as a green capping agent and reductant: photodynamic therapy

Maryam Rezaeizadeh [1], Mehdi Ranjbar [2], Abbas Pardakhty [3]*

[1]*Neuroscience Research Center, Institute of Neuropharmacology, Kerman University of Medical Sciences, Kerman, Iran*
[2]*Pharmaceutics Research Center, Institute of Neuropharmacology, Kerman University of Medical Sciences, Kerman, Iran*
[3]*Pharmaceutics Research Center, Kerman University of Medical Sciences, Kerman, Iran*

ABSTRACT

Objective (s): $SrCO_3$ nanoparticles could be used as new biomedical sources in magnetic resonance imaging as a promising noninvasive imaging modality for the preoperative staging of breast cancer and monitoring of tumor response to therapy. The present study aimed to synthesize SrCO3 nanostructures using microwave irradiation in the presence of honey as a green capping agent and reductant.

Materials and Methods: The optical properties of $SrCO_3$ nanostructures were investigated using ultraviolet-visible (UV-Vis) spectroscopy. $Sr(NO_3)$ $2.6H_{2O}$ and NaOH were applied as the starting reagents. Fructose (32.56-38.2%) and glucose (28.54-31.3%), which were the main carbohydrates found in honey, were not only involved in stabilization, but they also acted as the reducing agents in the production of $SrCO_3$ nanostructures. The produced nanostructures were characterized using X-ray diffraction analysis, Fourier transform infrared spectroscopy, scanning electron microscopy, and transmission electron microscopy.

Results: Method of synthesis and chemical reagents were observed to affect the structural parameters, crystallite size, product size, morphology, and antioxidant activity.

Conclusion: According to the results, honey could be used as a green capping agent and reductant for the synthesis of $SrCO_3$ nanostructures as a novel structure to co-deliver therapeutic agents using photo-thermal agents. Moreover, honey has significant potential for diagnostic and therapeutic purposes in the future.

Keywords: *Capping Agent, Drug Carriers, Photodynamic Therapy, $SrCO_3$ NPs*

How to cite this article

Rezaeizadeh M, Ranjbar M, Pardakhty A. Biosynthesis of $srco_3$ nanostructures with honey as a green capping agent and reductant: photodynamic therapy. Nanomed J. 2019; 6(2): 100-104. DOI: 10.22038/nmj.2019.06.0003

INTRODUCTION

Extensive research has recently been focused on the role and effects of fluorescence imaging and bimodal photodynamic therapy (PDT) materials against numerous human diseases and the food corruption caused by oxidative degradation [1-3]. Antioxidants, which are free radical inhibitors, have been considered more important than other materials. Therefore, evaluation of their inhibitory capacity has attracted the attention of researchers [4-6].

Despite their limitations, the chemical methods used to determine the PDT capacity of samples could be useful as they are simple and cost-effective [7-9]. Several methods are available to examine various PDT capacities and their efficacy in various cases, such as free radical regeneration [7, 10, 11], iron regenerative antioxidants [12], and oxygen radical absorption capacity [13, 14]. In PDT, visible light is applied to generate oxygen specimens [15, 16]. The cytotoxic and free radicals that selectively destroy rapidly growing cells as a stable free radical species have been widely recognized for the verification of antioxidant activity [17, 18]. PDT destroys cancer cells through the extraction of an unpredictable light sensor by non-harmful light [19, 20]. Moreover, ABTS as a chemical method assay determines antioxidant activity. In addition, ABTS is a practical test for aqueous media at various pH levels [21, 22].

Strontium is a soft, silver-yellow metal, which is relatively abundant in the Earth's crust and has special characteristics that make it an effective

* *Corresponding Author Email: mehdi.ranjbar@kmu.ac.ir*
Note. This manuscript was submitted on January 2, 2019; approved on February 29, 2019

compound for the long-term chronic treatment of postmenopausal osteoporosis [23, 24]. Strontium could be applied as an additive in the production of modern electric industries [25, 26], color television tubes [27], pigment production [28], and pyrotechnics [29]. In recent years, several synthesis techniques have been employed for the preparation of strontium oxide (SrO) and strontium carbonate ($SrCO_3$) structures, including microwave-assisted ultrasound [30], hydrothermal techniques [31], solvothermal techniques [32], and sol-gel process [33]. The energy of microwave waves has been used for the assessment of new chemical reactions, causing general changes in the kinetics (the theory of the speed of reactions) and selectivity of the reactions. The present study aimed to investigate the biosynthesis of $SrCO_3$ nanostructures using honey as a green capping and reductant agent in photodynamic therapy.

MATERIALS AND METHODS

Materials and Characterization

The chemical reagents used in the experiments included $Sr(NO_3)_2$ as the Sr precursor and NaOH as the pH regulator, which were of analytical grade and used without further purification. The honey used in the current research was obtained from Sirjan Mountains in Kerman province, Iran.

Table 1. Summary of Recent Studies Regarding Synthesis of $SrCO_3$ Nanostructures

Nanostructures	Synthesis Method	Particle Size	Ref.
$SrCO_3$	Methanol Solution	Sphere-like	[34]
Mesoporous $SrCO_3$	Hydrothermal Method	Rod-like	[35]
$SrCO_3$	Co-precipitation	Nanorods	[36]
Sr(OH)2 and $SrCO_3$	Ultrasonic Method	Particle	[37]
$SrCO_3$	Hydrothermal Method	Flower-like	[38]

To characterize the products, the X-ray diffraction (XRD) patterns were recorded using a Rigaku Dmax C III X-ray diffractometer and Ni-filtered Cu Ka radiation. Scanning electron microscopy (SEM) images were also obtained (SEM, Philips XL-30ESM), and the Fourier transform infrared (FT-IR) spectroscopy was recorded on a Nicolet Fourier Transform IR, (Nicolet 100 spectrometer) within the range of 500-4000 cm^{-1} using the KBr disk technique. In addition, the particle size and size distribution of the $SrCO_3$ nanostructures were determined via laser-light scattering (Mastersizer 2000 E, Malvern Instruments, UK).

Synthesis of the $SrCO_3$ Nanostructures

$SrCO_3$ structures were synthesized successfully via microwave irradiation. Approximately 0.63 millimole of $Sr(NO_3)_2$ was dissolved in 10 milliliters of 1:2 deionized water (DI):propylene glycol, and 10 milliliters of NaOH 2M was added to the solution for setting up 7.3<pH<8.2 under vigorous stirring (700 rpm) at the temperature of 50.

At the next stage, one milliliter of honey was dissolved in five milliliters of propylene glycol, which was added to the solution. The suspension was immediately loaded into a microwave Teflon container, and the reactions were performed using a microwave digestion system. The final product was dried in an oven at the temperature of 70 for 48 hr.In recent years, several studies have been focused on the synthesis of $SrCO_3$ nanostructures in drugs transfer. The summary of these studies is presented in Table 1.

Table 2. Reaction Conditions for Synthesis of $SrCO_3$ Nanostructures

No	Power (w)	Time (min)	Morphology	Size
1	150	15	Agglomeration	~5µm
2	350	12	Microparticle	~2.5µm
3	450	10	Nanoparticle	~650 nm
4	600	8	Rice-like	~200nm
5	750	5	Nanoparticle	~900nm
6	900	5	Microparticle	~1.5µm

RESULTS AND DISCUSSION

The reactions of all the samples were performed using a microwave digestion system (Table 2). The FT-IR spectrum of the synthesized $SrCO_3$ nanostructures at room temperature and after calcination at the temperature of 150 is depicted in Figs 1-a and 1-b, respectively.

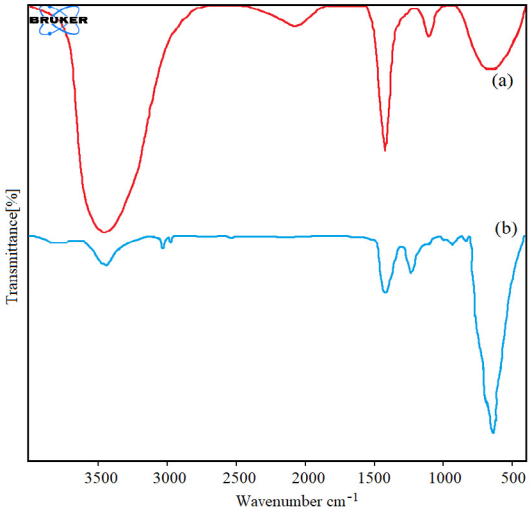

Fig 1. FT-IR Spectra of $SrCO_3$ Nanostructures; a) Room Temperature, b) after Calcination at Temperature of 150 °C

The broad absorption band within the range of 3000-3600 cm^{-1} matched the OH functional, which was associated with the activated surface to volume in the nanoparticles ratio rather than the bulk ones. In addition, the bands at 671, 958, 1170, and 1458 cm^{-1} corresponding to CO_3^{2-} were associated with the calcined $SrCO_3$ nanostructures.

Figs 2-a and 2-b show the XRD patterns and energy-dispersive X-ray spectroscopy (EDX), respectively for the third sample after calcination at the temperature of 150 °c.

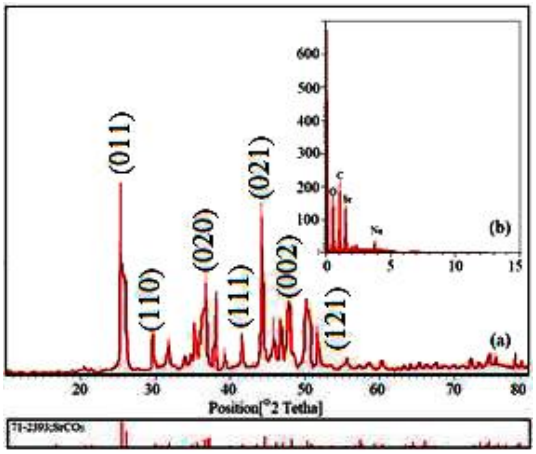

Fig 2. XRD Patterns of $SrCO_3$ Nanostructures for Sample Three after Calcination at Temperature of 150 °C

In Fig 2, (111), (220), and (311) are Miller indices, which were consistent with the orthorhombic structure of strontium carbonate with the space group (Pmcn), and a< 5.09>, b<8.35>, and c<5.99> were the network constants (JCPDS No.: 71-2393). To interpret the X-ray pattern, the correlation between the diffraction angle (2θ), wavelength of the X-ray beam (λ), and distance between each set of atomic planes of the crystal lattice (d) were calculated using Debye-Scherrer equation (Equation 1). As a result, the mean diameter of the crystallites (60-70 nm) was determined using the following formula:

$$D=k\lambda/\beta\cos(\theta) \qquad \text{Equation (1)}$$

where *D* is the mean crystallites size, *λ* shows the X-ray wavelength (1.54056 A°), *β* represents the full width at half maximum (FWHM), *ϑ* is the diffraction angle in the Bragg plane, *k* denotes the shape factor (0.9), and *EDX* shows the percentage of the element ratio of Sr:C:O in the SrCO3 nanostructures. In addition, energy dispersive X-Ray spectroscopy (EDS) was carried out on the $SrCO_3$ nanostructures in order to investigate the chemical composition and purity of the synthesized products. The presence of a negligible amount of Na in the samples was associated with the use of NaOH.

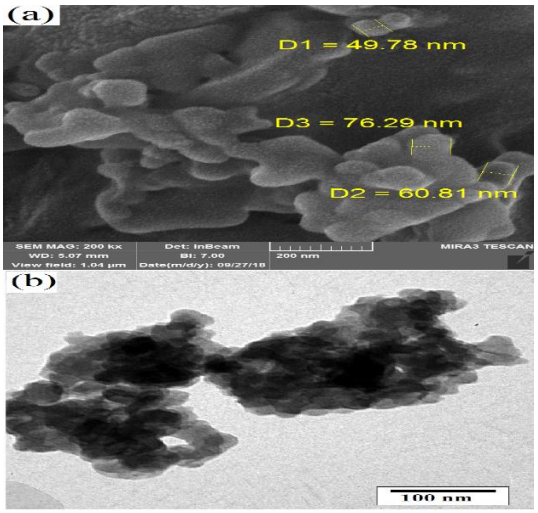

Fig 3. a) SEM and b) TEM of SrCO3 Nanostructures in Sample Three

To recognize the morphology and particle size distribution of the $SrCO_3$ nanostructures, SEM and TEM were performed on the prepared samples. As is depicted in Figs 3-a and 3-b, the sample of pure $SrCO_3$ nanostructures was composed of plate-like nanoparticles with the approximate diameters of 50-70 nanometers.

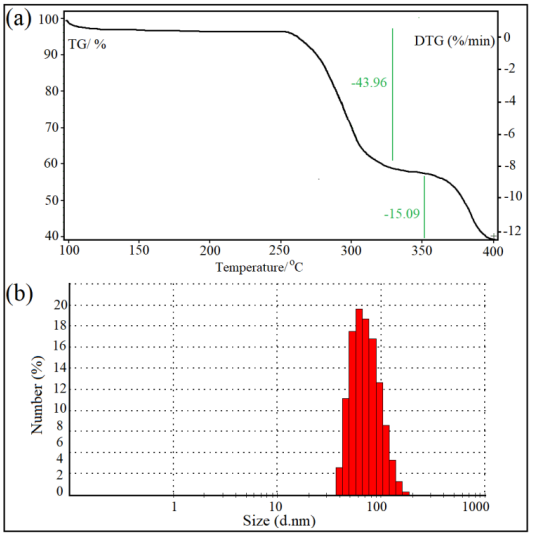

Fig 4. a) TGA Analysis and b) DLS Analysis of $SrCO_3$ Nanostructures in Sample Four

The results obtained by the thermogravimetric analyzer (TGA) regarding the $SrCO_3$ nanostructures are illustrated in Fig 4-a.

The TGA curve showed a number of degradation stages in the samples. Decomposition of the $SrCO_3$ nanostructures began at the temperature of 270 up to 330 with a free fall in the residual weight within the range of 43.96-15.09%. This could be attributed to the thermal decomposition of the covalent bond between Sr-C and C-O in the network of the $SrCO_3$ structure.

Dynamic laser scattering (DLS) was performed using Zetasizer HS3000 (Malvern Instruments, UK) at a detection angle of 90° and temperature of 25. In this process, the samples were dissolved in deionized water, homogenized, and filtered (0.22 µl) before transfer into a transparent cuvette for analysis. The DLS results regarding the $SrCO_3$ nanostructures indicated that the samples had a uniform size and low aggregation with the particle size of approximately 50-70 nanometers (Fig 4-b).

Optical Properties of the $SrCO_3$ Nanostructures

The optical properties of the nanomaterials were determined based on the measurements of UV-Vis spectroscopy. At the nanomaterial scale, the increased surface-to-volume ratio led to varied and unexpected physicochemical properties, which made the $SrCO_3$ nanostructures useful for biosensor and PDT applications, thereby potentially providing solutions to the problems associated with the current methods.

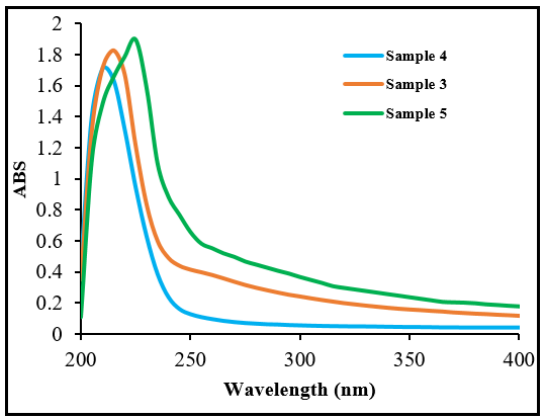

Fig 5. Room Temperature in UV-Vis Spectra of $SrCO_3$ Nanostructures

Fig 5 depicts the emissions centered at 210, 215, and 225 nanometers in the $SrCO_3$ nanostructure samples 3-5, respectively. The emission spectrum indicated a blue shift with a smaller particle size. Therefore, the synthesized nanoparticles could be presented as new nanomaterials in PDT. Due to the UV-Vis absorption of close to the area of 200 nanometers, the structure was considered super photocatalytic and had significant optical and photocatalytic properties.

CONCLUSION

PDT has been used more frequently compared to the other methods in this regard, and nanomaterials and nanocomposites have also been employed widely in clinical practices. Nanoscale materials are hoped to increase the effectiveness of PDT. According to the results of this study, the mean diameter of the $SrCO_3$ nanostructures was 60-70 nanometers based on the XRD pattern. Furthermore, the SEM and TEM results indicated that the $SrCO_3$ nanostructures were synthesized with uniform size distribution and emission peak of approximately 210-225 nanometers.

In this study, honey was used as a stabilizing and reduction agent in the production of the $SrCO_3$ nanostructures. The outcomes demonstrated the capability of these nanomaterials as a novel structure to co-deliver therapeutic agents using photothermal agents, which will have an enormous potential for future diagnosis and therapy.

ACKNOWLEDGMENTS

Hereby, we extend our gratitude to the Council of Pharmaceutics Research Center of the Institute of Neuropharmacology at Kerman University of Medical Sciences in Kerman, Iran for assisting us in this research project.

REFERENCES

1.Lucky S S, Soo KC, Zhang Y, Nanoparticles in photodynamic therapy. Chem Rev. 2015 ; 115 (4): 1990-2042.

2.Park YI, Kim H, Kyung C, Byeongjun Y, Kang L, Nohyun L, Yoonseok C, Wooram P, Daishun L, Kun N, Woo K, Moon S, Hong C, Hong S, Park S, Young Y, Yung Doug S, Sung H, Taeghwan H, Theranostic probe based on lanthanide-doped nanoparticles for simultaneous in vivo dual-modal imaging and photodynamic therapy. Adv Mater. 2012; 24(24): 5755-5761.

3.Bechet D, Serge RM, François G, Muriel A B, Photodynamic therapy of malignant brain tumours: a complementary approach to conventional therapies. Cancer Treat Res. 2014; 40(2): 229-241.

4.Punjabi A, Xiang W, Amira T, Mahmoud E, Hyungseok L, Yuanwei Z, Chao W, Zhuang L, Emory M. C, Chunying D, Gang H, Amplifying the red-emission of upconverting nanoparticles for biocompatible clinically used prodrug-induced photodynamic therapy. ACS nano. 2014; 8(10): 10621-10630.

5.Xu K, Yao H, Jinhui H, Zhou L, Zhou S, Pre-drug Self-assembled Nanoparticles: Recovering activity and overcoming glutathione-associated cell antioxidant resistance against photodynamic therapy. Free Radic Biol Med. 2018; 124(20): 431-446.

6.Youssef Z, Valérie H, Ludovic C, Philippe A, Moussaron A, Baros F, Toufaily J, Hamieh T, Carmes T, Frochot C, Titania and silica nanoparticles coupled to Chlorin e6 for anti-cancer photodynamic therapy. Free Radic Res. 2018; 22(6): 115-126.
7.Gamaleia N F, Shton I O, Gold mining for PDT: Great expectations from tiny nanoparticles. Photodiagnosis Photodyn Ther. 2015; 12(2): 221-231.
8.Moritz M N O, Joyce L S, Gonçalves I, Linares J, Kleber T , Semi-synthesis and PDT activities of a new amphiphilic chlorin derivative. Photodiagnosis Photodyn Ther. 2017; 17(3): 39-47.
9.Oniszczuk A, Karolina A, Wojtunik K, Tomasz O, Kamila K, Show M, The potential of photodynamic therapy (PDT)—Experimental investigations and clinical use. Biomed. Pharmacother. 2016; 83(4): 912-929.
10.Liu Y, Meng X, Bu W, Upconversion-based photodynamic cancer therapy. COORDIN CHEM REV. 2019; 379(15): 82-98.
11.Yurt F, MineInce S, Gokhan Colak, Kasim O, Ozge E, Hale M, Soylu C, Gunduz B, Avci C, Caliskan K, Investigation of in vitro PDT activities of zinc phthalocyanine immobilised TiO2 nanoparticles. Int J Pharm.2017; 524(15): 467-474.
12.Nyanhongo G S, Christoph S, Roland L, Nugroho P, Georg M.G, An antioxidant regenerating system for continuous quenching of free radicals in chronic wounds. Eur J Pharm Biopharm. 2013; 83(3): 396-404.
13.Prior R.L, Oxygen radical absorbance capacity (ORAC): New horizons in relating dietary antioxidants/bioactives and health benefits. J FUNCT FOODS. 2015; 18(3): 797-810.
14.Trivittayasil V, Hiromi K, Toshihiko S, Mizuki T, Mito K, Junichi S, Simultaneous estimation of scavenging capacities of peach extract for multiple reactive oxygen species by fluorescence fingerprint method.Food Chem. 2017; 232(1): 523-530.
15.O'Mahoney P,Neil H, Kenny W, Tom A, Browne S, Ewan E, Show M, A novel light source with tuneable uniformity of light distribution for artificial daylight photodynamic therapy. Photodiagnosis Photodyn Ther. 2018; 23(34): 144-150.
16.Vignion-DewalleA.-S, Gregory B, EliseT, Claire V, Laurent M, Serge M, Show M, Photodynamic therapy for actinic keratosis: Is the European consensus protocol for daylight PDT superior to conventional protocol for Aktilite CL 128 PDT, J. Photochem. Photobiol. 2017; 174(3): 70-77.
17.DaiY,Xiuli Z, Yanying Hu, Zhang Y,Liu M, Quantum chemical calculation of free radical substitution reaction mechanism of camptothecin. J Mol Graph Model. 2018; 84 (2): 174-181.
18.Mason R P, and Ganini D, Immuno-spin trapping of macromolecules free radicals in vitro and in vivo – One stop shopping for free radical detection. Free Radic Biol Med. 2019; 131(1): 318-331.
19.Niu N, Zhe Z, Xiao Z, Chen S, Photodynamic therapy in hypoxia: Near-infrared-sensitive, self-supported, oxygen generation nano-platform enabled by upconverting nanoparticles. Chem Eng J.2018; 352(15): 818-827.
20.Wysocka-Król K, Olsztyńska S, Janus [G, Plesch] A, Plecenik H, Podbielska J, , Nano-silver modified silica particles in antibacterial photodynamic therapy. Appl Surf Sci. 2018; 461(15): 260-268.
21.Diao J, Feng B, Ying W, Qianqian H, XiXu H, Zhang Q, Yanqing W, Engineering of pectin-dopamine nano-conjugates for carrying ruthenium complex: A potential tool for biomedical applications. J J Inorg Biochem. 2019; 191(4): 135-142.
22.Pan Y, Hua M, Liping H, Juan H, Yan L, Ziwei H, Li [J, Yang] A, Graphene enhanced transformation of lignin in laccase-ABTS system by accelerating electron transfer. Enzyme Microb Technol. 2018; 119 (3): 17-23.
23.Glisic M, Qiang F, Zhe L, Meng-Lin L, Shuang-Qing Z, Phytoestrogen supplementation and body composition in postmenopausal women: A systematic review and meta-analysis of randomized controlled trials. Maturitas, 2018; 115(25): 74-83.
24.Paschalis E P, Gamsjaeger N, Hassler A, Fahrleitner-P, Dobnig H, Stepan JJ, I.Pavo E, eKlaushofer K, Vitamin D and calcium supplementation for three years in postmenopausal osteoporosis significantly alters bone mineral and organic matrix quality. Bone. 2017; 95(3): 41-46.
25.Achillas C, Aidonis D, Lakovou E, Thymianidis[a] M, Tzetzis D[a], A methodological framework for the inclusion of modern additive manufacturing into the production portfolio of a focused factory. JMSY. 2015; 37(1): 328-339.
26.Schmidt M,Marion M, David B, Dimitri D, Tino H, Konrad W, Ludger O, Frank V, Gideon N, Laser based additive manufacturing in industry and academia. CIRP Ann Manuf Technol. 2017; 66(2): 561-583.
27.Amed S, Occupational dermatitis in the manufacture of color television tubes. American Am J Contact Dermat. 1997; 8(4): 222-224.
28.Venkatachalam M, Hélène M,Laurent D, Mireille F[ac], Production of pigments from the tropical marine-derived fungi Talaromyces albobiverticillius: New resources for natural red-colored metabolites. J Food Compos Anal. 2018; 70(2): 35-48.
29.Steinhauser G, Johannes H, Sterba M, Foster F, Grass M, Heavy metals from pyrotechnics in New Years Eve snow. Atmos Chem Phys. 2008; 42(37): 8616-8622.
30.Pasquet V, Jean-René C, Firas F, Valérie T, Jean-Marie P, Jean B, Bérard R, Kaas B, Serive T, Jean-Paul C, Laurent P, Show M, Study on the microalgal pigments extraction process: Performance of microwave assisted extraction. Process Biochem. 2011; 46(1): 59-67.
31.Xia X, Jiang-ping T, Yong-jin M, Xiu-li W, Chang-dong G, Xin-bing Z, Self-supported hydrothermal synthesized hollow Co3O4 nanowire arrays with high supercapacitor capacitance. J Mater Chem A. 2011; 21(25): 9319-9325.
32.Ni Z, Masel R, Rapid production of metal– organic frameworks via microwave-assisted solvothermal synthesis. Comm. 2006; 128(38): 12394-12395.
33.Macwan D, P.N. Dave, Chaturvedi S, A review on nano-TiO2 sol–gel type syntheses and its applications. J Mater Sci. 2011; 46(11): 3669-3686.
34.Li L, Rongyi L, Email Z, Tong Q, Feng M, Facile synthesis of $SrCO_3$ nanostructures in methanol/water solution without additives. Nanoscale Res Lett. 2012; 7(4): 305-315.
35.Zhu, W, Guanglei Z, Jing L, Qiang Z, Xianglan P, Shenlin Z, Hierarchical mesoporous $SrCO_3$ submicron spheres derived from reaction-limited aggregation induced "rod-to-dumbbell-to-sphere" self-assembly. CrystEngComm. 2010; 12(6): 1795-1802.
36.Arumugam D, Mathavan T, Jeshua L, Archana J, Murugan P, Selvaraj S, Umapathy S, Mukul G, Gunadhor S, Michael J, Milton A, Growth Mechanism of Pine-leaf-like Nanostructure from the Backbone of SrCO3 Nanorods using LaMer's Surface Diffusion: Impact of Higher Surface Energy (γ= 38.9 eV/nm2){111} Plane Stacking Along 110(γ= 3.4 eV/nm2) by First-Principles Calculations. Cryst Growth Des. 2017; 17(2): 6394-6406.
37.Alavi MA, Morsali A, Syntheses and characterization of $Sr(OH)_2$ and $SrCO_3$ nanostructures by ultrasonic method. Ultrason Sonochem. 2010; 17(1):132-138.
38.Yang L, Deqing C, Limin W, Ge G, Huilou S, Facile synthesis of porous flower-like SrCO3 nanostructures by integrating bottom-up and top-down routes. Mater Lett. 2016; 167(15): 4-8.